Switching a Perpendicular Ferromagnetic Layer by Competing Spin Currents

Qinli Ma, Yufan Li, D. B. Gopman, Yu. P. Kabanov, R. D. Shull, and C. L. Chien

Phys. Rev. Lett. **120**, 117703 — Published 16 March 2018

DOI: 10.1103/PhysRevLett.120.117703

Switching a perpendicular ferromagnetic layer by competing spin currents

Qinli Ma[1*†], Yufan Li[1†], D. B. Gopman[2], Yu. P. Kabanov[2,3], R. D. Shull[2], and C. L. Chien[1*]

[1]Department of Physics and Astronomy, Johns Hopkins University, Baltimore, MD 21218, USA

[2]National Institute of Standards and Technology, Gaithersburg, MD 20899, USA

[3]Institute for Solid State Physics, RAS, Chernogolovka, Moscow distr., 142432, Russia

Abstract

An ultimate goal of spintronics is to control magnetism via electrical means. One promising way is to utilize a current-induced spin-orbit torque (SOT) originating from the strong spin-orbit coupling in heavy metals and their interfaces to switch a single perpendicularly magnetized ferromagnetic layer at room temperature. However, experimental realization of SOT switching to date requires an additional in-plane magnetic field, or other more complex measures, thus severely limiting its prospects. Here we present a novel structure consisting of two heavy metals that delivers competing spin currents of opposite spin indices. Instead of just canceling the pure spin current and the associated SOTs as one expects and corroborated by the widely accepted SOTs, such devices manifest the ability to switch the perpendicular CoFeB magnetization solely with an in-plane current without any magnetic field. Magnetic domain imaging reveals selective asymmetrical domain wall motion under a current. Our discovery not only paves the way for the application of SOT in non-volatile technologies, but also poses questions on the underlying mechanism of the commonly believed SOT-induced switching phenomenon.

†: these author contribute equally

* corresponding author: Qinli Ma qma7@jhu.edu, Chia Ling Chien: clchien@jhu.edu

Switching of ferromagnets is central to many magnetic memory applications from high-density magnetic recording to magnetic random access memories (MRAM) (1,2). A ferromagnetic (FM) entity can always be, and for a long time could only be, switched by a magnetic field. The discovery of spin transfer torque (STT) enabled current switching of FM entities in nanostructures, whereby spin polarized currents generated in a pinned FM layer in a FM-metal-FM (spin valve) or FM-insulator-FM (magnetic tunnel junction) device exerts a torque on the magnetization of a second (free) FM layer (3-6). However, the high STT switching current density through the device is undesirable.

The advent of spin-orbit torque (SOT) allows the prospects of electrical switching of a single FM layer with perpendicular magnetic anisotropy (PMA) by a peripheral current (7-12). The general structure of a perpendicular SOT device is a HM/FM/I trilayer, as shown in Fig. 1a, where the FM layer (e.g., Co, CoFeB), sandwiched between a heavy metal (HM), e.g., Pt and W, and a light oxide (I), e.g., AlO_x and MgO, acquires PMA. Due to the spin Hall effect (SHE) and the interfacial Rashba effect, a charge current $\boldsymbol{J}$ (in the x-direction) gives rise to a pure spin current $\boldsymbol{J_s} \propto \theta_{SH}\boldsymbol{J} \times \boldsymbol{\sigma}$ and a spin accumulation in the out-of-plane (z) direction, respectively**,** with a spin index $\boldsymbol{\sigma}$ in the direction perpendicular to both $\boldsymbol{J_s}$ and $\boldsymbol{J}$**,** that is along the y-direction (7-9). The effective spin Hall angle θ_{SH} specifies the charge-to-spin conversion efficiency. Heavy metals with large θ_{SH}, such as Pt, Ta and W (10-14), are important for SOT devices, in which the anomalous Hall effect (AHE) generates a transverse voltage in proportion to the orientation of the perpendicularly magnetized layer (Fig, 1b). As illustrated in Fig. 1a and in contrast to STT devices, the charge current passes peripheral to, and not through, the magnetic multilayers.

Switching of a PMA layer by SOT was first demonstrated by Miron *et al.* in 2011 and Liu *et al.* in 2012 in Pt/Co/AlO_x (10,11). We have obtained similar results in W/CoFeB/MgO (See supplementary material I for SOT switching in W/CoFeB/MgO). However, to date, SOT switching in HM/FM/I multilayers cannot occur *unless* an external magnetic field $\mu_0\boldsymbol{H_x}$ is also applied along the current direction. The field direction, parallel or antiparallel to $\boldsymbol{J}$, dictates the states with up or down magnetization at large current. (Fig. 1c). Higher $\mu_0\boldsymbol{H_x}$ reduces the switching current density, but switching cannot occur at any current density without a magnetic field. The requirement of a

magnetic field severely diminishes the prospects of SOT switching. By altering the anisotropy of the FM layer, using an asymmetrical geometrical shape or magnetic exchange bias, switching without a field has been demonstrated in prototype devices (15-19), but scaling these measures up for technologically relevant device arrays may present unique challenges.

Present understanding of SOT switching in HM/FM/I is based on the Dzyaloshinskii-Moriya interaction (DMI) and the domain wall (DW) motion driven by SOT (20-25). The DMI at the HM/FM interface causes a Néel DW with a certain chirality. For a series of hypothetical up ($\uparrow$)/down($\downarrow$) domains along the *x*-direction with magnetization pointing in the *+z/-z* directions, spins within the DWs rotate in the vertical *xz* plane with a single chirality that is set by the sign of the DMI constant. Under a current in the *x*-direction, the SOT causes motion of the DW. Theoretical and experimental studies in the last few years have concluded that the relevant SOT for HM/FM/I, has two terms, namely the field-like torque $\boldsymbol{\tau_{FL}} = a\boldsymbol{M} \times \boldsymbol{\sigma}$ and the anti-damping-like torque $\boldsymbol{\tau_{DL}} = b\boldsymbol{M} \times (\boldsymbol{\sigma} \times \boldsymbol{M})$, where mainly the latter drives the DWs (20-23). The Landau-Lifshitz-Gilbert (LLG) equation including the SOT is

$$\frac{\partial \boldsymbol{M}}{\partial t} = -\gamma \boldsymbol{M} \times H + \frac{\alpha}{M} \boldsymbol{M} \times \frac{\partial \boldsymbol{M}}{\partial t} + a\boldsymbol{M} \times \boldsymbol{\sigma} + b\boldsymbol{M} \times (\boldsymbol{\sigma} \times \boldsymbol{M}) \qquad (1)$$

where the first two terms are the precession term and the damping term. The corresponding effective fields of the two terms of SOT, $\boldsymbol{H_{FL}} \sim \boldsymbol{\sigma}$ and $\boldsymbol{H_{DL}} \sim \boldsymbol{\sigma} \times \boldsymbol{M}$ are in the *xy*-plane along the *y* and the *x* axes, respectively, shown in Fig. 1a. For DWs with one chirality, the effective field $\boldsymbol{H_{DL}}$ acting on the $\uparrow\downarrow$ and $\downarrow\uparrow$ DWs are also opposite. Consequently, the SOTs influence both $\uparrow\downarrow$ and $\downarrow\uparrow$ DWs to move in the *same* direction and with the *same* speed ($\mathbf{v}_{\uparrow\downarrow} = \mathbf{v}_{\downarrow\uparrow}$), thus resulting in no net change in the overall magnetization, thus, no switching. The external magnetic field $\boldsymbol{H_x}$ along the current direction $\boldsymbol{J}$ changes the relative orientation of the central DW moments, causing $\mathbf{v}_{\uparrow\downarrow} \neq \mathbf{v}_{\downarrow\uparrow}$ and enabling $+\boldsymbol{M}$ with one polarity and $-\boldsymbol{M}$ with the opposite polarity of current. Thus, the external field $\boldsymbol{H_x}$ breaks the degeneracy of up-down and down-up DWs with regard to the SOT, and causes unequal DW motion that accomplishes switching,

even for nanostructures (24). Simulation using Eq. (1) reveals these essential results, including the necessity of an external field $\boldsymbol{H_x}$ (22-25).

To date, SOT switching and the validity of Eq. (1) have been extensively studied only in HM/FM/I with *one* HM layer, involving spin current of one spin index $\boldsymbol{\sigma}$. Since the strengths *a* and *b* of the two SOT terms in Eq.(1) scale with θ_{SH}, efficient switching relies on a HM with a large θ_{SH}, such as Pt or W, whose main contrast lies in the opposite sign of θ_{SH} and the opposite SOT. In this work, we experimentally explore the implications of Eq. (1) by employing a *second* HM with an opposite spin index $\boldsymbol{-\sigma}$, such as Pt/W/CoFeB/MgO, as shown in Fig. 1d. Since the two SOT terms are linear in $\boldsymbol{\sigma}$, the second HM with an opposite θ_{SH} would generate a pure spin current of opposite $\boldsymbol{\sigma}$. This should be expected to only reduce the net spin current and the associated SOT, resulting in a larger switching current density. With a sufficiently thick second HM, the net spin current and SOT of the HM bilayer complex would vanish, resulting in no current switching. In short, the effect of the second HM with opposite θ_{SH} is trivial and counter-productive as LLG simulation of Eq. (1) readily predicts. Contrary to conventional predictions, we observe effective SOT switching in Pt/W/CoFeB/MgO heterostructures. Not only is a net SOT evident in this material with nominally opposing SOTs, current induced switching occurs without any superimposed magnetic field, i.e., zero-field switching (ZFS), a feat that has eluded all HM/FM/I with a single HM. These results suggest a hitherto unknown mechanism due to *competing* spin currents that enables ZFS.

We used magnetron sputtering with normal incidence for the fabrication of the multilayers, except the W layer, which was made by oblique (off-axis) sputtering to capture the β-W phase. The direction of oblique sputtering also defines an important in-plane structural symmetry within W/CoFeB/MgO, with CoFeB as $Co_{40}Fe_{40}B_{20}$, in which the direction perpendicular to the off-axis direction is denoted as $\alpha = 0°$ and 180°. All the films were deposited on Si/SiO_2 substrate. The multilayers were then annealed in vacuum at 300 ºC for 1 hour to acquire the PMA of CoFeB. We use optical lithography to pattern multilayers into Hall bar structures, where the current channel is 20 μm (width) × 120 μm (length) and the voltage channel width of 10 μm, with the current direction along various directions specified by α. The oblique sputtered W layer has a thickness difference of

about 1 nm over a lateral distance of 3 cm. The W thickness variation in the actual samples is within 10^{-3} nm, i.e., indistinguishable from a uniform layer.

We first discuss the results of Hall bars patterned in the direction of $\alpha = 0°$. The results of W(1)/CoFeB(1)/MgO(2) (in nm) are shown in Fig. 1b and 1c. The AHE loops are centered at $\mu_0 H_z = 0$, regardless of the current value (Fig. 1b). Consistent with the SOT switching phenomena, current induced switching of this device requires an external field $\mu_0 \boldsymbol{H_x}$, where $+\mu_0 H_x$ (parallel to $+I$) leads to the $+M$ state at large $+I$, and the opposite for $-\mu_0 H_x$ (Fig. 1c). However, the results of Pt(3.8)/W(1)/CoFeB(1)/MgO (in nm), are very different. The AHE loops of Pt/W/CoFeB/MgO are distinctively off-center with the loop shifts to one side (Fig. 1e) as if under a perpendicular field $\mu_0 \boldsymbol{H}_\perp$, which increases linearly with current density J (See Supplemental Material II for AHE of Pt/W/CoFeB/MgO devices). At a sufficiently large current, purely electrical switching occurs at zero field (Fig. 1f), i.e., ZFS. In fact, this sample continues to exhibit the same SOT switching under modest fields $\mu_0 \boldsymbol{H_x}$ of up to about ±10 mT. The switching current density between samples is similar, although the switching current in W/CoFeB/MgO (Fig. 1c) is smaller than that in Pt/W/CoFeB/MgO (Fig. 1f) due to different metal layer thicknesses.

To determine the relative contributions of Pt and W, we measured a series of samples of Pt(3)/W(t_W = 0.7 - 1.6)/CoFeB(1)/MgO with a constant Pt(3) layer and various thicknesses of the W layer. As shown in Fig. 2a, ZFS (solid symbols), each with a sizable $\mu_0 \boldsymbol{H}_\perp$, has been observed in the range of about $0.7 < t_W < 1.3$ nm. Samples outside this thickness range (open symbols) do not exhibit ZFS. In another series, we varied the Pt layer thickness in Pt(t_{Pt} = 1.5 - 4.5)/W(1)/CoFeB(1)/MgO and observed ZFS with $1.5 < t_{Pt} < 3.8$ as shown in Fig. 2b. The ratio $\mu_0 \boldsymbol{H}_\perp/J$, measures the efficiency of ZFS. As shown in Fig. 2a and 2b, the $\mu_0 \boldsymbol{H}_\perp/J$ value varies systematically with t_W and t_{Pt} with a maximal $\mu_0 \boldsymbol{H}_\perp/J$ of 8 mT/(10^{11}A/m^2) occurring at Pt(3)/W(1)/CoFeB(1)/MgO from the two series. There is no ZFS with $\mu_0 \boldsymbol{H}_\perp/J \approx 0$ and switching requires $\mu_0 \boldsymbol{H_x}$ as in HM/FM/I. When the conventional SOT reduces (Fig. 2e), J_c dose not increase (Fig. 2c). In fact, J_c has the lowest value in Pt(3)/W(1)/CoFeB(1)/MgO, the structure with robust ZFS and maximal $\mu_0 \boldsymbol{H}_\perp/J$. For ZFS, the thicknesses of W ($0.8 < t_W < 1.3$) are smaller than those of Pt ($1.5 < t_{Pt} < 3.8$), because of the higher spin current injection efficiency

from the W layer, which is in contact with the CoFeB layer. One might suspect that the second HM of Pt in Pt/W/CoFeB/MgO may alter the DMI, or cause other effects from the additional Pt/W interface. We note the DMI constants of W/CoFeB and Pt/CoFeB have the same sign and similar values (26-28).

We have also performed harmonic measurements (29-31) to quantitatively measure the effective H_{DL} and H_{FL}, through $H_{DL(FL)}=2(\frac{dV_{2\omega}}{dH_{x(y)}})/(\frac{d^2V_{\omega}}{d^2H_{x(y)}})$, where $V_{\omega,2\omega}$ are first and second harmonic Hall signal, $H_{x,y}$ are in-plane magnetic field along and perpendicular to the current direction. The results of Pt(3)/W(t_W = 0.7 - 1.6)/CoFeB(1)/MgO are shown in Fig. 2e . First of all, both SOTs in Pt/W/CoFeB/MgO are about one order of magnitude smaller than those with W and Pt alone (25,26), reflecting the reduced net spin current, consistent with conventional SOT phenomenology. Both $\boldsymbol{\tau_{FL}}$ and $\boldsymbol{\tau_{DL}}$ vary systematically with t_W from positive to negative as t_W increases. Importantly, both $\boldsymbol{\tau_{FL}}$ and $\boldsymbol{\tau_{DL}}$ cross zero at about t_W = 1 nm. Thus, the most efficient ZFS switching occurs in Pt(3)/W(1)/CoFeB(1)/MgO where all the key quantities for conventional SOTs, including $\boldsymbol{\tau_{FL}}$, $\boldsymbol{\tau_{DL}}$, and the effective θ_{SH}, are *vanishingly* small. This indicates that the ZFS in Pt(3)/W(1)/CoFeB/MgO is not adequately captured by the conventional SOT mechanism whose strength is evaluated by $\boldsymbol{\tau_{FL}}$ and $\boldsymbol{\tau_{DL}}$, but instead by a new mechanism, identified by $\mu_0\boldsymbol{H}_{\perp}/J$.

To reveal the magnetization switching under the electric current, we use magnetic optical Kerr effect (MOKE) imaging on Pt(2.5 nm)/W(1.0 nm)/CoFeB/MgO to directly observe magnetic domains and DW motion during current switching from -*M* to +*M* with -*I* (Fig. 3a), and from +*M* to –*M* with +*I* (Fig. 3b). In these images, the up (down) or +*M* (-*M*) domains have black (white) contrast. Under -*I* of increasing magnitude, the images proceed in the order of 1, 2, 3, 4, 5, where the +*M* domains expand asymmetrically. Because of the multiple domains, DW motions occur at multiple locations, with subsequent domain consolidation. The ↑ ↓ DW on the right side moves opposite to the conventional current direction, while the ↓ ↑ DW on the left side moves much slower. This disparity in the DW speeds of the two types of DWs, in the absence of a magnetic field, is the key feature of Pt/W/CoFeB/MgO that leads to ZFS. The reverse process is shown in Fig. 3b under +*I* of increasing magnitude shown by the images in the order of A

to E, and similar asymmetrical DW motion was observed. It is noted that, the DWs tend to expand as current increases (See Supplemental Material IV for Domain expansion under current), suggesting a perpendicular field associated with the current in Pt/W. By including the $\mu_0 \boldsymbol{H}_\perp/J$ in eq. (1), together with the conventional SOT described by $\boldsymbol{M} \times (\boldsymbol{\sigma} \times \boldsymbol{M})$, the asymmetric motion of ↑↓ and ↓↑ DWs along current direction, thus the ZFS, can be well reproduced by LLG equation (See Supplemental Material IV for the simulation of asymmetric domain wall motion, which including Ref 25, 27, 32).

We use current pulses of 11.8 mA in magnitude and 50 μs in width to reveal the consequence of each current pulse. In the top row of Fig. 3c, we show the MOKE images of the same region after 3 successive current pulses. In the lower row we highlight in yellow the domain after the previous current pulse, revealing the asymmetrical domain growth from this current pulse. From these images one concludes that the highest DW speed, occurring at the tip of the down-up DW after each current pulse, is about 3 cm/s at this low current density. An increase in current density dramatically increases the DW speed as necessary for devices application (22, 23).

We next discuss the ZFS switching anisotropy. In W/CoFeB/MgO, as in other HM/FM/I, the external field $\mu_0 \boldsymbol{H}_x$ along the current direction sets the switching sense of the $\pm M$ states as shown in Fig. 1c. The current channel may be patterned along any direction α within the CoFeB plane with no discernable difference. This isotropy is also realized in W/CoFeB/MgO samples with the oblique sputtered W layer. However, in Pt/W/CoFeB/MgO (Fig. 1f) that exhibits ZFS, current of opposite polarities gives the opposite states of $\pm \boldsymbol{M}$, thus with a distinct anisotropy. We patterned Pt/W/CoFeB/MgO with 10 μm channel width along different directions in the film plane, with $\alpha = 90°$ denoted as the off-axis sputtering direction. The angular dependence of the switching current is shown in Fig. 4a, where the switching current mid-points for up-to-down and down-to-up are denoted as I_C(U-D) (solid circles) and I_C(D-U) (open circles) respectively. The remnant Hall resistance $R_H(0)$ that measures the degree of reversal is also shown. The angular dependence of I_C(U-D), I_C(D-U), and $R_H(0)$ shows a two-fold symmetry with $\alpha = 0°$ as the symmetry axis. Deterministic switching occurs with nearly the same switching current of ±6.7 mA ($J_c = 1.3 \times 10^{11}$ A/m^2) within a wide range of angle of about ± 60° centered at $\alpha = 0°$, and with the opposite M at $\alpha = 180°$. In

contrast, only partial switching with a smaller $R_H(0)$, requiring a larger current of ±7.1 mA ($J_c = 1.4\times10^{11}$ A/m^2), occurs near the perpendicular direction of $\alpha = 90°$ and 270°. The anisotropy axis is likely set by the oblique sputtering direction for the W layer. Off-axis sputtering is known to promote grain growth in the oblique direction, which causes the in-plane anisotropy (33, 34).

In addition to Pt/W/CoFeB/MgO, we have also observed ZFS in Pt/Ta/CoFeB/MgO but not in Ta/W/CoFeB/MgO. Since Ta and W both have negative θ_{SH} and Pt has positive θ_{SH}, these results further reaffirm the essential feature of two spin currents with opposite $\boldsymbol{\sigma}$ rather than multilayer structure. To further demonstrate the essential features of two spin currents of opposite spin index, in Pt/W/CoFeB/MgO with ZFS, we insert a 1-nm Au layer between Pt and W as in Pt/Au/W/CoFeB/MgO, where the much weaker charge-to-spin conversion of Au effectively reduces the spin current from Pt (35,36). As a result, ZFS no longer occurs, and switching requires a field. To address the Oersted field due to the charge current, we capped the Pt/W/CoFeB/MgO with Ta(1 nm)/Au(3 nm), the current through which would compensate the Oersted field from the bottom Pt/W. We found ZFS remains intact thus excluding Oersted field as a possible cause. These observations reaffirm the essential features of competing spin currents. We note a pure spin current, with a direction, a magnitude, and a spin index $\boldsymbol{\sigma}$, is *not* a vector. But in the present model of SOT, the effect of the spin current has been incorporated into a spin flux vector with direction $\boldsymbol{\sigma}$ and a magnitude that scales with θ_{SH}, as in the field-like torque $(a\boldsymbol{M}\times\boldsymbol{\sigma})$ and the anti-damping-like torque $(b\boldsymbol{M}\times(\boldsymbol{\sigma}\times\boldsymbol{M}))$ in Eq. (1). To accomplish ZFS one needs create additional in-plane anisotropy on magnetic unit through geometrical shape (15-17) or exchange bias (18,19). We show in this work, the competing spin currents can also facilitate a new mechanism, experimentally revealed as $\mu_0\boldsymbol{H}_\perp \propto J$, that causes asymmetric motion of up-down and down-up DWs along current direction, and performs ZFS at sufficiently large current.

In summary, we demonstrate a novel switching mechanism via two spin currents of opposite spin indices in Pt/W/CoFeB/MgO and similar structures. Instead of merely cancelling the spin current and SOT as the present model would indicate, we show that the competing spin currents generate an effective SOT with an effective perpendicular field that can switch a PMA layer without any applied magnetic field. We show that the

present model of SOT does not provide a viable scheme for multiple spin currents, a new avenue for magnetization switching and DW motion.

Acknowledgments

This work was supported by the U.S. Department of Energy, Basic Energy Science, Award Grant No. DE-SC0009390. Y. L. was supported in part by STARnet, a SRC program sponsored by MARCO and DARPA. Q. M. was supported in part by SHINES, an EFRC funded by the US DOE Basic Energy Science award number SC0012670. Q.M thanks Weiwei Lin for helpful discussions on magnetization switching related to domain wall motion.

Reference:

1. C. Chappert, A. Fert, and F. N. Van Dau, *Nature Mater*. **6**, 813 (2007).
2. N. Locatelli, V. Cros, and J. Grollier, *Nature Mater*. **13**, 11-20 (2014).
3. J. C. Slonczewski, *J. Magn. Magn. Mater*. **159**, L1 (1996); ibid.**195**, L261 (1999).
4. L. Berger, *Phys. Rev. B* **54**, 9353 (1996); J. Appl. Phys. **81**, 4880 (1997).
5. J. C. Sankey, et al. *Nature Phys*. **4**, 67 (2008).
6. S. S. P. Parkin, M. Hayashi, and L. Thomas, *Sciences*. **320**, 190-194 (2008).
7. A. Manchon, and S. Zhang, *Phys. Rev. B* **79**, 094422 (2009).
8. M. D. Stiles and Z. Zangwill, Phys. Rev. B **66**, 104407 (2002)
9. V. P. Amin and M. D. Stiles, Phys. Rev. B **94**, 104419 (2016)
10. I. M. Miron, et al. *Nature* **476**, 189-193 (2011).
11. L. Liu, et al. *Phys. Rev. Lett*. **109**, 096602 (2012).
12. L. Liu, et al. *Sciences* **336**, 555-558 (2012).
13. Q. Hao, and G. Xiao, *Phys. Rev. Appl*. **3**, 034009 (2015).
14. X. C. Zhang, et al. *J. Appl. Phys*. **115**, 17C714 (2014)
15. G. Yu, et al. *Nature nanotech*. **9**, 548-554 (2014).
16. L. Youa, et al. *PNAS* **112**, 10310-10315(2015).
17. C. K. Safeer, et al. *Nature nanotech*. **11**, 143-143 (2016).
18. S. Fukami, et al. *Nature Mater*. 15, 535–541 (2016).
19. Y. –C. Lau, et al. *Nature Nano.* 11, 758–762 (2016).
20. O. J. Lee et al., *Phys. Rev. B* **89**, 024418 (2014).
21. C. O. Avciet al., *Phys. Rev. B* **89**, 214419 (2014).
22. S. Emori et al., *Nature Mater*. **12**, 611 (2013).
23. P. P. J. Haazen et al., *Nature Mater*. **12**, 299 (2013).
24. M. Baumgartner et al.,Nat. Nanotech. 12, 980 (2017)
25. A. V. Khvalkovskiy et al., *Phys. Rev. B* **87**, 020402(R) (2013).
26. K. Di et al., Appl. Phys. Lett. 106, 052403 (2015)
27. A. K. Chaurasiya et al., Scientific Reports 6, Article number: 32592 (2016)
28. I. Gross et al., *Phys. Rev. B* **90**, 064413 (2016).
29. J. Kim et al., Nature Materials, 12, 240–245 (2013)
30. J. Cho et al., *Nature Communs*, **6**, 7635 (2015).
31. K. Garello et al., *Nat. Nanotech.* 8, 587 (2013)
32. [reference in Supplemental Material not already in paper] Q. L. Ma et al. *Appl.Phys. Lett.* **101**, 122414 (2012).

33. R. N. Tait et al. *J. Vac. Sci. Technol. A*. **10**, 1518 (1992)

34. R. D. McMichael et al., *J. Appl. Phys*. **88**, 5296 (2000)

35. M. Isasa et al., Phys Rev B. **91**, 024402 (2015).

36. H. J. Zhang et al., Sci. Rep. **4**, 4844 (2014)

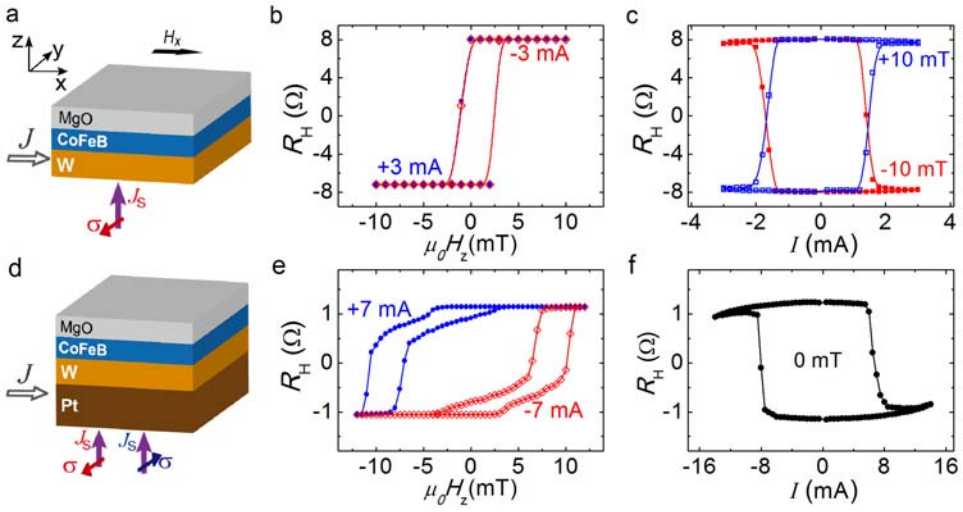

Figure 1. Structures and current-induced switching behaviors in CoFeB with PMA, patterned with α = 0º. (a) Conventional SOT switching in W(1)/CoFeB(1)/MgO(1.8), (b) anomalous Hall effect (AHE) effect under +3 mA (blue solid circles) and -3 mA (open diamond circles), and (c) switching requiring a magnetic field. (d) Competing SOT effects of Pt/W/CoFeB/MgO. (e) AHE under positive and negative current, (f) Current induced magnetization switching requiring no magnetic field.

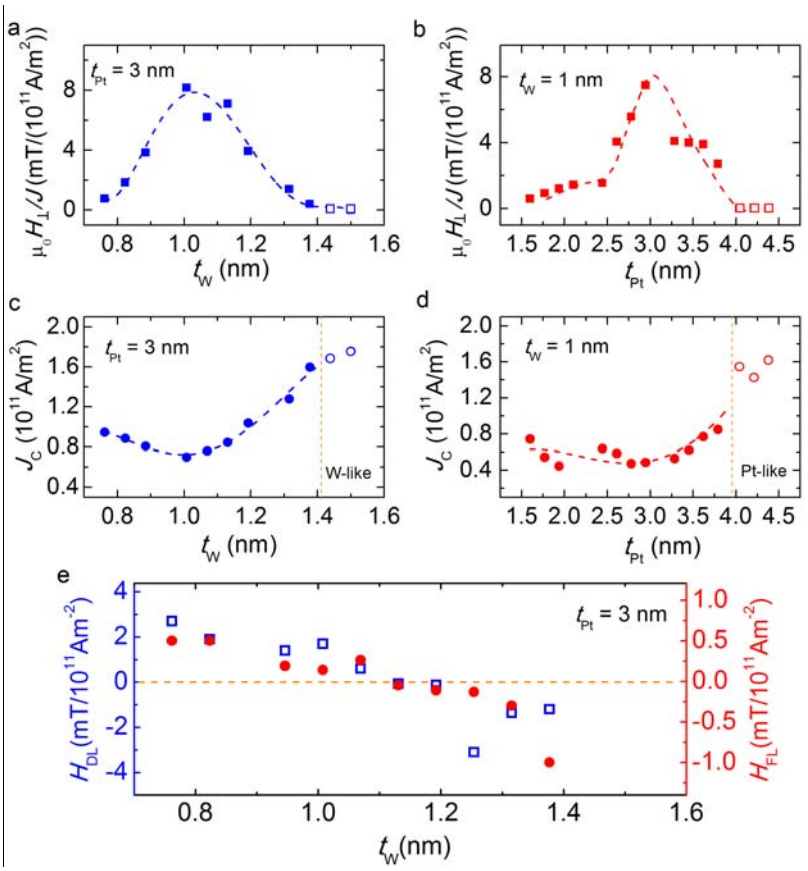

Figure 2. SOT switching dependence on Pt and W thickness in Pt/W/CoFeB/MgO. In Pt(3)/W(t_W)/CoFeB(1)/MgO(1.8) with a fixed t_{Pt} = 3 nm (a) $\mu_0 H_\perp/J$ and (c) switching density J_C. In Pt(t_{Pt})/W(1)/CoFeB(1)/MgO(1.8) with a fixed t_W = 1 nm, (b) $\mu_0 H_\perp/J$ and (d) J_C. In (c) and (d) the solid and open symbols are for $\mu_0 H_x$ = 0 and 7 mT, respectively. (e) H_{FL} (solid circles) and H_{DL} (open squares) obtained from harmonic measurements for Pt(3.0)/W(t_W)/CoFeB(1)/MgO(1.8). These two series show Pt(3)/W(1.1)/CoFeB(1)/MgO(1.8) has the maximal $\mu_0 H_\perp/J$, minimal J_C, and $H_{FL} \approx 0$ and $H_{DL} \approx 0$.

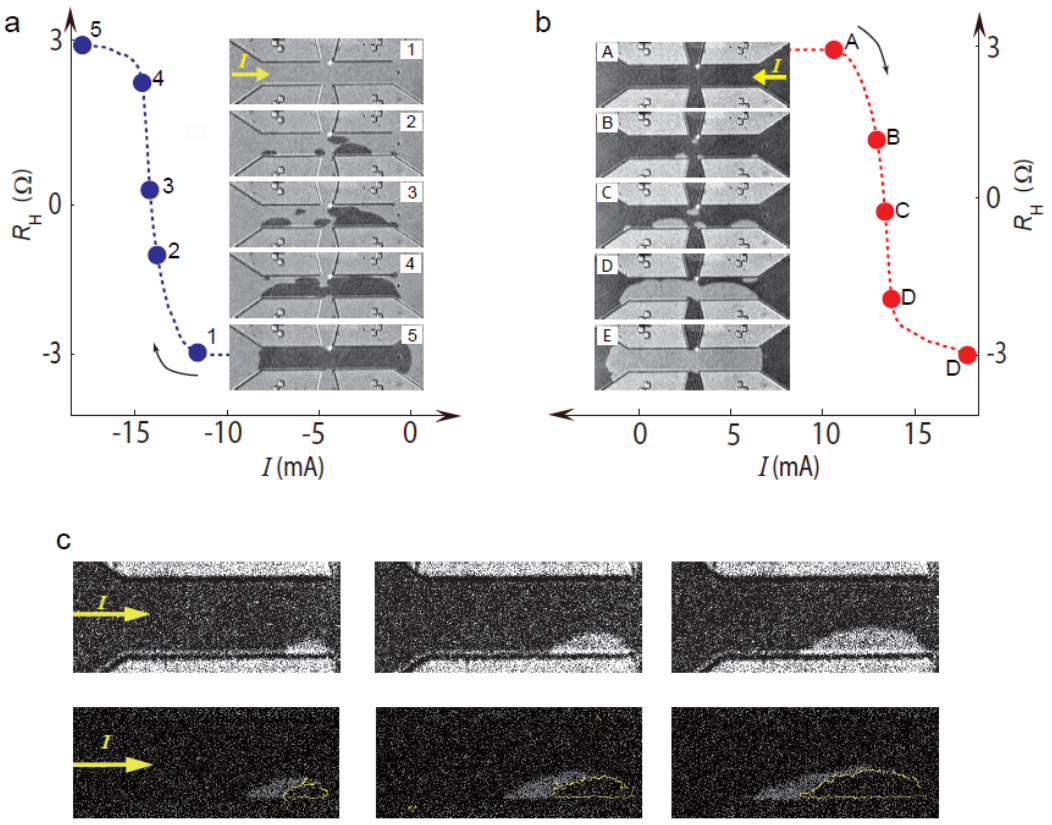

Figure 3. MOKE images of current switching in Hall bar of Pt(2.5)/W(1.0)/CoFeB(1) for (a) increasing -I in the order of 1, 2, 3... and (b) increasing +I in the order of A, B, C... (c) Images after successive current pulses asymmetrically enlarging the domains at one end. In the lower panel, the yellow boundaries show the domains just before the current pulse, illustrating the contribution of the one current pulse.

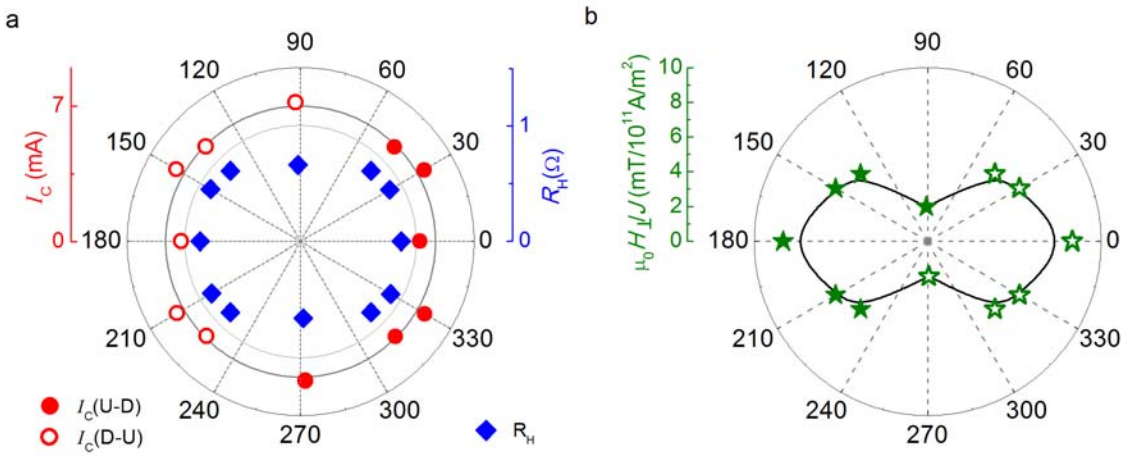

Figure 4. Anisotropy of ZFS in Pt(3)/W(1.1)/CoFeB(1)/MgO(2) (in nm). (a) Angular dependence of the R_H values, I_C and (b) $\mu_0 H_\perp/J$ values, where the solid and open circles indicate magnetization switching from up-to-down and down-to-up respectively.